Supporting Information

Analysing Oxygen Reduction Electrocatalysis on Transition Metal doped Niobium oxide (110)

Christina Susan Abraham, [†, a] Megha Anand, [†, a] Sara R. Kelly, [b] Zhenbin Wang, [a] and Jens K. Nørskov [*, a]

a. Center for Catalysis Theory, Technical University of Denmark, Fysikvej Building 311, 2800 Kongens Lyngby, Denmark

b. Department of Chemical Engineering, Stanford University, Stanford, CA 94305, USA

† These authors contributed equally.

* Corresponding author Corresponding author: jkno@dtu.dk

Sl. No.	Content	Page No.
1.	Fundamentals of ORR (Reaction pathway)	S4
2.	Computational Methods	S4
3.	Surface Pourbaix Analysis	S6
4.	Analyzing the stability of doped system in terms of the formation energies at standard conditions	S7
	4.1 Range of O chemical potential	S7
	4.2 Oxygen molecule chemical potential	S7
	4.3 Enthalpy of formation of stable form of dopant	S8
5.	Structural modification of doped niobium pentoxide systems, M-$Nb_{31}O_{80}$	S11
6.	Linear Scaling relations	S12
	6.1 Linear scaling relations between G_{OOH^*} vs G_{OH^*}	S12
	6.2 Linear scaling relations between G_{O^*} vs G_{OH^*}	S13
7.	OH binding energy of IrO_2(110)	S16
	References	S17

List of figures

Sl. No.	Content		Page No.
S1	Crystal structures of Nb_2O_5	. . . . .	S5
S2	Side view of the pristine stoichiometric metal doped Nb_2O_5 (110) surface. Surface and sub-surface doping sites are considered for TM atoms. (b) Calculated formation energy per O atom (eV) of transition metal doped niobium oxide systems.	. . . . .	S6
S3	Range of allowed O chemical potentials	. . . . .	S7
S4 (a)	**Side view of ORR adsorbate:** OOH adsorbed on Rh, Re and Pt doped $Nb_{32-x}O_{80}$ where the binding site is the dopant (c_1)	. . . . .	S12
S4 (b)	**Side view of ORR adsorbate**: OH adsorbed on Cr, Mn (c_1) and Co (c_2) doped $Nb_{32-x}O_{80}$.	. . . . .	S12
S5	**Side view of ORR adsorbate**: O adsorbed on Co, Zn, Rh, Au and Cu doped $Nb_{32-x}O_{80}$ where the binding site is the Nb metal atom site (c_2)	. . . . .	S13
S6	Free energies versus applied potential (vs RHE) for different surface coverages on Ir-$Nb_{31}O_{80}$ (110) at pH = 0.	. . . . .	S14
S7	**Calculated TDOS and PDOS** of (a) $Nb_{32}O_{80}$ (110), (b) Mo-$Nb_{31}O_{80}$ (c) 2Mo-$Nb_{30}O_{80}$.	. . . . .	S15
S8	**Kinetic volcano model** for the 4e- ORR process at 0.8 V_{RHE}	. . . . .	S15
S9	**Comparing free energies of different OH coverage surfaces sampled for IrO_2 (110)** (pH = 0)	. . . . .	S16

List of tables

Sl. No.	Content		Page No.
S1	Free energy of reference molecules	. . . . .	S4
S2	Enthalpy of formation and free energy of formation of the oxide form of the dopant metal at standard conditions	. . . . .	S9
S3	Bond distances between the dopant transition metal and the surrounding O atoms in the M-$Nb_{31}O_{80}$ systems (M = dopant transition metals).	. . . . .	S11
S4	Differential OH binding energy at high coverage on IrO_2 (110)	. . . . .	S16

1. Fundamentals of ORR (Reaction pathway)

The binding free energy (ΔG_{ads}) of an ORR intermediate on a catalyst slab is calculated relative to the pristine slab (with no adsorbate), H_2O (g) and H_2 (g). Thus,

$$\Delta G_{ads} = \Delta E_{ads} + \Delta G_{correction}$$

where ΔE_{ads} represents the relative DFT energy of the adsorbate-catalyst system and $\Delta G_{correction}$ is the free energy correction taken from reference.[1]

Table S1 | Free energy of reference molecules optimized in a 20 × 20 × 20 Å^3 cell.

Molecule	E	ZPE	TS	$\int C_p dT$	ZPE-TS+$\int C_p dT$	$\Delta G_{correction}$	G
H_2O	-14.691	0.567	0.675	0.104	-0.004		-14.695
H_2	-7.046	0.271	0.407	0.09	-0.046		-7.092
OOH* [1]		0.464	0.096	0.058	0.426	0.365	
O* [1]		0.093	0.035	0.023	0.081	0.039	
OH* [1]		0.354	0.1	0.053	0.307	0.288	

In addition to the entropic and zero-point energy corrections, solvation correction is also considered. Explicit solvation decreases the binding energies of OOH* and OH* by 0.40 eV and 0.15eV [2] respectively. The change in binding energy for O* is negligible.

2. Computational Methods

In the present study we selected Nb_2O_5 with space groups: C2/m [12], P1[1], P$\bar{1}$[2], P2[3], I4/mmm [139] and $P2_12_12_1$ [19]. All these materials have an E_{hull} lower than 0.15ev/atom. E_{hull} is used as a criterion to estimate the stability of the candidate material and thereby predict its synthesizability.[3] The systems have similar electronic energies. The band gap of the tetragonal Nb_2O_5 crystal system is the lowest in comparison to the rest of the reported Nb_2O_5 crystal systems in Materials project[†1]and so, for further analysis, the tetragonal crystal Nb_2O_5 system was used. Hubbard U correction values where considered for select 3d transition metal dopant systems.

[†] It is worth noting that the semi-local DFT used in Material project data tends to severely underestimate bandgaps.

Materials Id	Space group	Crystal system	Structure
mp-680944	P1 [1]	Triclinic	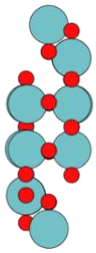
mp-766361	P1 [2]	Triclinic	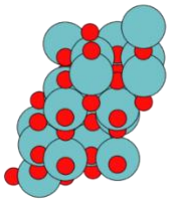
mp-581967	P2 [3]	Monoclinic	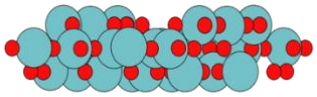
mp-556048	**I4/mmm [139]**	**Tetragonal**	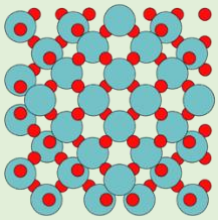
mp-776896	P212121 [19]	Orthorhombic	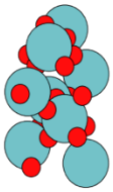

Fig. S1 | Crystal structures of Nb_2O_5. For further analysis the tetragonal crystal system (highlighted in green) is used.

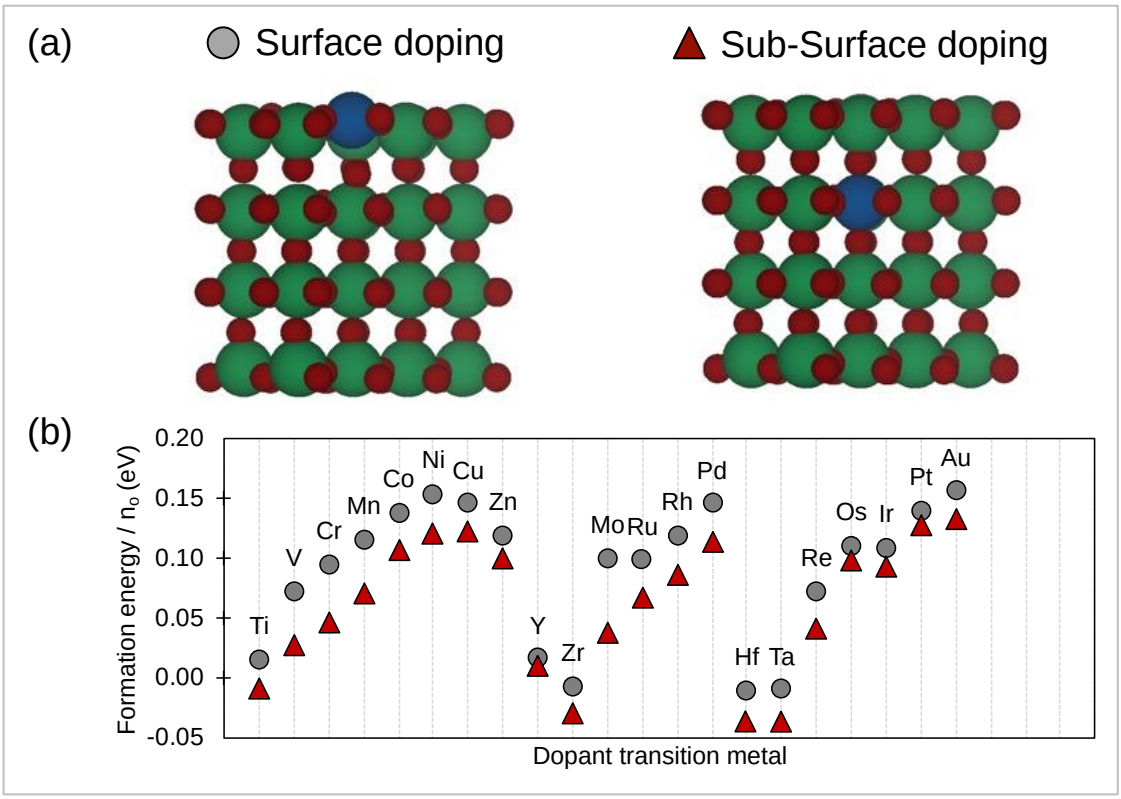

Fig . S2 | (a) Side view of the pristine stoichiometric metal doped Nb_2O_5 (110) surface. Surface and sub-surface doping sites are considered for TM atoms. Colour code: Nb (green), oxygen (maroon) and TM dopant (blue). (b) Calculated formation energy per O atom (eV) of transition metal doped niobium oxide systems. Circle and triangle markers corresponds to surface and sub-surface doping sites respectively.

3. Surface Pourbaix Analysis

Under ORR conditions, the oxide system might differ from its initial stoichiometric pristine form. It is therefore important to analyze the coverage of the catalyst surface. Surface Pourbaix analysis gives a good approximation of surface coverage under ORR reaction conditions. [4] Considering a metal surface M with * representing the site of adsorption in its pristine state, O_xH_y the ORR adsorption intermediates (x and y are the number of oxygen and hydrogen atoms respectively), k_B is the Boltzmann constant, and T is the temperature, then associated free energy change for adsorption of O_xH_y intermediates is given by:

$$\Delta G(U, pH) = G_{s-O_xH_y^*} - G_{S^*} - xG_{H_2O} + (2x - y)\left(\frac{1}{2}G_{H_2} - U_{SHE} - 2.303k_bTpH\right)$$

4. Analyzing the stability of doped system in terms of the formation energies

4.1 Range of O chemical potential

The method described in this section has been explained in detail by Reuter et. al.[5] The Gibbs free energy of bulk niobium oxide $g^{bulk}_{Nb_2O_5}$ can be expressed as follows, where the chemical potential of oxygen can vary under ORR conditions:

$$g^{bulk}_{Nb_2O_5} = 2\mu_{Nb} + 5\mu_O$$

$\frac{1}{5}$ 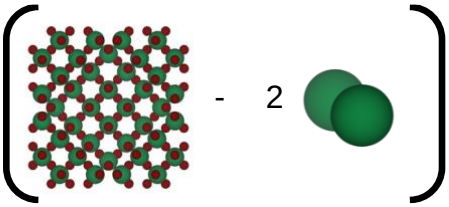 $\leq \mu_{O_2} \leq$  $\frac{1}{2}E^{total}_{O_2}$

Fig. S3 | Range of allowed O chemical potentials.

In low oxygen potential environment:

$$\min[\mu_O(T,P)] = \frac{1}{5}\left(g^{bulk}_{Nb_2O_5}(0,0) - 2g^{bulk}_{Nb}(0,0)\right)$$

where, $g^{bulk}_{Nb_2O_5}$ and g^{bulk}_{Nb} are the Gibb's free energy of bulk Niobium oxide and metallic Niobium. In high oxygen potential environment:

$$\max[\mu_O(T,P)] = \frac{1}{2}E^{total}_{O_2}$$

where, $E^{total}_{O_2}$ is the total energy of free, isolated O_2 molecule.

For our purpose, we consider only the high oxygen potential since there is constant supply of molecular oxygen during the ORR experiments.

4.2 Oxygen molecule chemical potential

The chemical potential of oxygen molecule $\mu_{O_2(g)}$ is derived from the standard free energy change of the reaction (equation (a)) in two steps:

$$\frac{1}{2}O_2(g) + H_2(g) \leftrightarrow H_2O(l) \qquad \text{(a)}$$

First we take the experimental standard free energy change of equation (a). It is -2.46eV as shown in equation (b) [6]

$$\Delta G^0_{H_2O(l)} = G^0_{H_2O(l)} - \frac{1}{2}G^0_{O_2(g)} - G^0_{H_2(g)} = -2.46\text{eV} \qquad \text{(b)}$$

Next we compute the chemical potential of water as follows,

$$\mu_{H_2O(l)} = \mu_{H_2O(g)} = \left(E^{H_2O(g)}_{DFT} + ZPE_{H_2O(g)} - TS^0_{H_2O(g)}\right) \qquad \text{(c)}$$

Combining the values from equations (a) and (b), the chemical potential of oxygen molecule is approximated as:

$$\mu_{O_2(g)} = 4.92 + 2\left(E_{DFT}^{H_2O(g)} + ZPE_{H_2O(g)} - TS^0_{H_2O(g)}\right) - 2\left(E_{DFT}^{H_2(g)} + ZPE_{H_2(g)} - TS^0_{H_2(g)}\right) \quad \text{(d)}$$

As we mentioned earlier, we are interested in the O-rich environment and use the value of O potential from equation (d) in the formation energy calculations.

4.3 Enthalpy of formation of stable form of dopant

To calculate the formation energies of the doped Nb_2O_5 systems, we require μ_M, chemical potential of the dopant metal, M. For this the $\Delta H_f^{M_xO_y}$, enthalpy of formation of the stable oxide form of the dopant metal at standard conditions is needed. We have $\Delta H_f^{M_xO_y}$ values from Wagman et al.[7] We first calculate the $\Delta G_f^\circ / n_M$ (where n_M = number of metal atoms in the formula) for different stoichiometries in which a metal exists in its oxide form (M_xO_y). The metal oxide with the lowest value of $\Delta G_f^\circ / n_M$ or the free energy of formation per metal atom at standard conditions is used as the reference. For some of the oxides, the free energy of formation data is unavailable in the reference paper. We approximate their ΔG_f° by adding the entropic contribution from molecular oxygen to the ΔH_f° of that oxide (equations shown below) from the same reference. It is assumed that metal, M(s) and the $M_xO_y(s)$ do not contribute to the entropy [$xM(s) + y/2O_2(g) \rightarrow M_xO_y(s)$]. At 1 bar pressure and 298.15K temperature, the entropy of O_2 is 205.138 $J^{-1}mol^{-1}$. Thus, the free energy of formation of a metal oxide is attained as:

$$\Delta G_f^\circ = \Delta H_f^\circ - T\,(-\Delta S_f^\circ\, O_2)$$

$$\Delta G_f^\circ = \Delta H_f^\circ - 298.15\text{ K}\,(-205.138\ J^{-1}mol^{-1})$$

$$\Delta G_f^\circ = \Delta H_f^\circ + 61161.8947\ Jmol^{-1}$$

$$\Delta G_f^\circ = \Delta H_f^\circ + 61.162\ KJmol^{-1}$$

The values of ΔG_f° and ΔH_f° marked in red are systems where the values are calculated using the above equation. The system highlighted in green in Table S2 is the most stable form among other oxide forms under standard conditions.

Table S2 | Enthalpy of formation and free energy of formation of the oxide form of the dopant metal at standard conditions.

Metal Oxide	ΔG_f° (kJmol^{-1})	$\Delta G_f^\circ/n_M$ (kJmol^{-1})	ΔH_f° (kJmol^{-1})	$\Delta H_f^\circ/n_M$ (kJmol^{-1})	$\Delta H_f^\circ/n_M$ (eV)
			Titanium		
TiO(α)	-495.00	-495.00	-519.70	-519.70	-5.39
TiO_2(anatase)	-884.50	-884.50	-939.70	-939.70	-9.74
TiO_2(brookite)	-880.64	-880.64	-941.80	-941.80	-9.76
TiO_2(rutile)	-889.50	-889.50	-944.70	-944.70	-9.79
Ti_2O_3	-1434.20	-717.10	-1520.90	-760.45	-7.88
Ti_3O_5	-2317.40	-772.47	-2459.40	-819.80	-8.50
			Vanadium		
VO	-404.20	-404.20	-431.80	-431.80	-4.48
V_2O_3	-1139.30	-569.65	-1218.80	-609.40	-6.32
V_2O_4(α)	-1318.30	-659.15	-1427.20	-713.60	-7.40
V_2O_5	-1419.50	-709.75	-1550.60	-775.30	-8.04
V_3O_5	-1803.00	-601.00	-1933.00	-644.33	-6.68
V_4O_7	-2456.00	-614.00	-2640.00	-660.00	-6.84
			Chromium		
CrO_2	-536.84	-536.84	-598.00	-598.00	-6.20
CrO_3	-497.76	-497.76	-589.50	-589.50	-6.11
Cr_2O_3	-1058.10	-529.05	-1139.70	-569.85	-5.91
Cr_3O_4	-1408.68	-469.56	-1531.00	-510.33	-5.29
			Manganese		
MnO	-362.90	-362.90	-385.22	-385.22	-3.99
MnO_2	-465.14	-465.14	-520.03	-520.03	-5.39
Mn_2O_3	-881.10	-440.55	-959.00	-479.50	-4.97
Mn_3O_4	-1283.20	-427.73	-1387.80	-462.60	-4.79
			Cobalt		
CoO	-214.2	-214.2	-237.94	-237.94	-2.47
Co_3O_4	-774	-258	-891	-297	-3.08
			Nickel		
NiO	-211.70	-211.70	-239.70	-239.70	-2.48
Ni_2O_3	-397.76	-198.88	-489.50	-244.75	-2.54
			Copper		
CuO	-129.7	-129.7	-157.3	-157.3	-1.63
Cu_2O	-146	-73	-168.6	-84.3	-0.87
			Zinc		
ZnO	-318.30	-318.30	-348.28	-348.28	-3.61

Metal	ΔG_f° (kJmol^{-1})	$\Delta G_f^\circ/n_M$ (kJmol^{-1})	ΔH_f° (kJmol^{-1})	$\Delta H_f^\circ/n_M$ (kJmol^{-1})	$\Delta H_f^\circ/n_M$ (eV)
Yttrium					
Y_2O_3	-1816.60	-908.30	-1905.31	-952.66	-9.87
Zirconium					
ZrO_2	-1042.79	-1042.79	-1100.56	-1100.56	-11.41
Molybdenum					
MoO_2	-533.01	-533.01	-588.94	-588.94	-6.10
MoO_3	-667.97	-667.97	-745.09	-745.09	-7.72
Ruthenium					
RuO_2	-243.84	-243.84	-305	-305	-3.16
RuO_4	-116.98	-116.98	-239.3	-239.3	-2.48
Rhodium					
Rh_2O_3	-251.3	-125.6	-343.0	-171.5	-1.8
Palladium					
PdO	-54.82	-54.82	-85.4	-85.4	-0.89
Hafnium					
HfO_2	-1088.20	-1088.20	-1144.70	-1144.70	-11.86
Tantalum					
Ta_2O_5	-1911.20	-955.60	-2046.00	-1023.00	-10.60
Tungsten					
WO_2	-533.89	-533.89	-589.69	-589.69	-6.11
WO_3	-764.03	-764.03	-842.87	-842.87	-8.74
Rhenium					
ReO_2	-368	-368	-429.16	-429.16	-4.45
ReO_3	-513.26	-513.26	-605	-605	-6.27
Re_2O_7	-1066	-533	-1240.1	-620.05	-6.43
Osmium					
OsO_3	-191.96	-191.96	-283.7	-283.7	-2.94
OsO_4 (yellow)	-304.9	-304.9	-394.1	-394.1	-4.08
OsO_4 (white)	-303.7	-303.7	-385.8	-385.8	-3.99
Iridium					
IrO_2	-212.94	-212.94	-274.1	-274.1	-2.84
Platinum					
Pt_3O_4	-40.68	-13.56	-163	-54.33	-0.56

5. Structural modification of doped niobium pentoxide systems, M-$Nb_{31}O_{80}$ (M = dopant transition metals)

Table S3 | Bond distances between the dopant transition metal and the surrounding O atoms in the M-$Nb_{31}O_{80}$ systems (M = dopant transition metals).

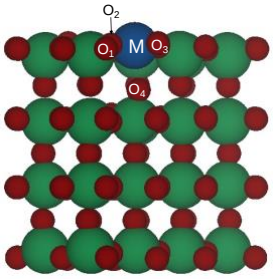

DOPED SYSTEM	Bond distance (Å)			
	O_1-M	O_2-M	O_3-M	O_4-M
$Nb_{32}O_{80}$	**2.249**	**2.009**	**1.959**	**1.798**
Ti-$Nb_{31}O_{80}$	2.174	2.016	1.951	1.761
V-$Nb_{31}O_{80}$	2.361	2.053	1.804	1.666
Cr-$Nb_{31}O_{80}$	2.653	1.943	1.789	1.654
Mn-$Nb_{31}O_{80}$	2.338	1.938	1.822	1.658
Co-$Nb_{31}O_{80}$	2.306	1.897	1.992	1.695
Ni-$Nb_{31}O_{80}$	2.171	2.03	2.033	1.736
Cu-$Nb_{31}O_{80}$	2.005	1.913	1.943	2.277
Zn-$Nb_{31}O_{80}$	2.178	2.051	2.174	2.038
Y-$Nb_{31}O_{80}$	2.325	2.237	2.277	2.17
Zr-$Nb_{31}O_{80}$	2.242	2.100	2.081	1.963
Mo-$Nb_{31}O_{80}$	2.216	1.928	1.866	1.735
Ru-$Nb_{31}O_{80}$	2.112	1.952	1.96	1.781
Rh-$Nb_{31}O_{80}$	2.103	2.084	1.994	1.804
Pd-$Nb_{31}O_{80}$	2.112	1.976	2.040	2.116
Hf-$Nb_{31}O_{80}$	2.187	2.071	2.062	1.935
Ta-$Nb_{31}O_{80}$	2.171	1.989	1.96	1.801
W-$Nb_{31}O_{80}$	2.165	1.914	1.853	1.745
Re-$Nb_{31}O_{80}$	2.125	1.881	1.890	1.768
Os-$Nb_{31}O_{80}$	2.075	1.934	1.939	1.793
Ir-$Nb_{31}O_{80}$	2.06	1.967	1.972	1.84
Pt-$Nb_{31}O_{80}$	2.063	1.989	1.988	1.881
Au-$Nb_{31}O_{80}$	2.079	2.001	2.033	2.741

6. Linear Scaling relations

The ORR intermediates adsorption on the doped niobium pentoxide was analyzed on both the dopant site (c_1) as well as the niobium metal site (c_2). When fitting the linear scaling relation, the most stable site for the ORR intermediate adsorption was used. The data points corresponding to ΔG_{OOH^*} > 4.98 eV, ΔG_{O^*} > 4.86 eV and ΔG_{OH^*} > 2.2 eV are shown in the plot but while fitting the scaling lines, these points are excluded.[8-10]

6.1 Linear scaling relations between G_{OOH^*} vs G_{OH^*}

Data points higher than ΔG_{OOH^*} = 4.98eV and ΔG_{OH^*} = 2.2 eV are neglected and the slope is fixed at 1.

The data points corresponding to Rh, Re, and Pt doped $Nb_{32-x}O_{80}$ (c_1) are neglected since the adsorbate OOH breaks to form O* and OH (refer figure S4 (a)).

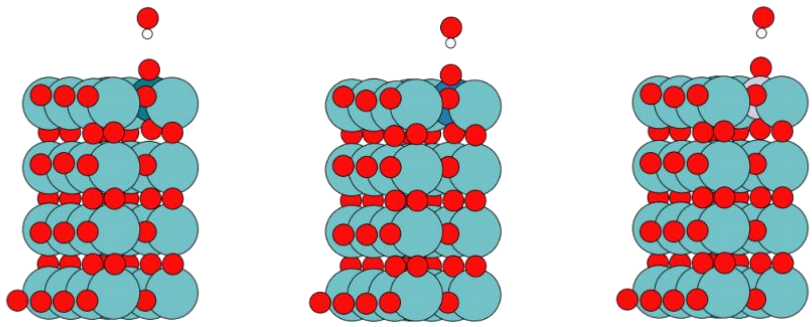

Rh-$Nb_{31}O_{80}$ Re-$Nb_{31}O_{80}$ Pt-$Nb_{31}O_{80}$

Fig S4(a) | Side view of ORR adsorbate: OOH adsorbed on Rh, Re and Pt doped $Nb_{32-x}O_{80}$ where the binding site is the dopant (c_1)

The data point corresponding to Cr (c_1), Mn (c_1) and Co (c_2) doped $Nb_{32-x}O_{80}$ are also neglected. It is seen to be set off from the scaling line. This could be due to structural modification of the doped system during OH adsorption (refer figure S4 (b)) where the Cr, Mn and Co gets off the surface with sub-surface oxygen atoms.

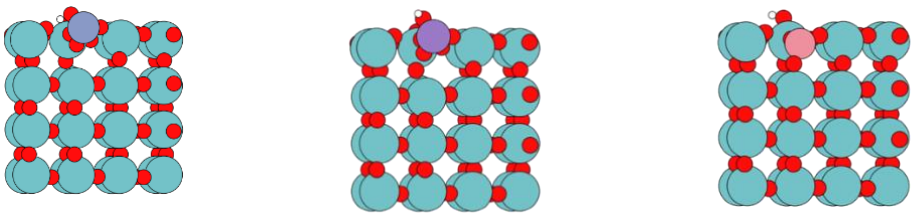

Cr-$Nb_{31}O_{80}$ Mn-$Nb_{31}O_{80}$ Co-$Nb_{31}O_{80}$

Fig S4(b) | Side view of ORR adsorbate: OH adsorbed on Cr(c_1), Mn (c_1) and Co (c_2) doped $Nb_{32-x}O_{80}$.

6.2 Linear scaling relations between G_{O^*} vs G_{OH^*}

Data points higher than ΔG_{O^*} = 4.86eV and ΔG_{OH^*} = 2.2 eV are neglected and the slope is fixed at 2.

The data points corresponding to Co, Zn, Rh and Au doped $Nb_{32-x}O_{80}$ (c_2) are neglected from the linear scaling relations between ORR adsorbates, G_{O^*} vs G_{OH^*}. This is because the adsorbate O binds on the non-metal site (O) of the $Nb_{32-x}O_{80}$ surface (refer figure S5). The data points corresponding to Zn doped $Nb_{32-x}O_{80}$ (c_1) and Cu doped $Nb_{32-x}O_{80}$ (c_2) are neglected since adsorbate O binds on the non-metal site (O) of the $Nb_{32-x}O_{80}$ surface and forms O_2 (refer figure S5).

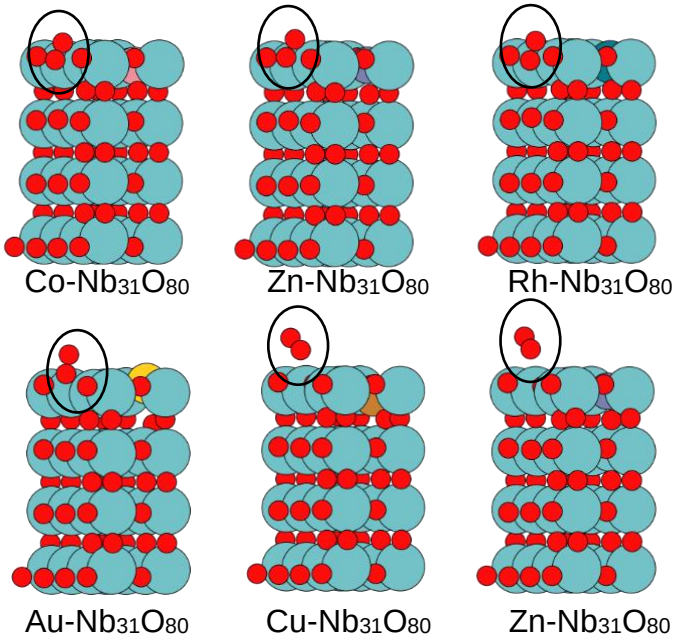

Fig S5 | Side view of ORR adsorbate: O adsorbed on Co, Zn, Rh, Au and Cu doped $Nb_{32-x}O_{80}$ where the binding site is the Nb metal atom site (c_2)

While all the data points are represented in the Figure 3 (data points corresponding to adsorption on both dopant site as well as Niobium metal site), the deviation of few doped systems from the doped Nb_2O_5 scaling line can be attributed to:

1. The doped Nb_2O_5 systems with free energy values of OOH*, O* and OH* higher than 4.98, 4.86 and 2.2 eV respectively are excluded while fitting the linear scaling relation.
2. The scaling relation corresponds only to the most stable site of adsorption.
3. The slope of the scaling lines has also been fixed at 1 and 2 in case of ΔG_{OOH^*} vs ΔG_{OH^*} and ΔG_{O^*} vs ΔG_{OH^*} respectively for ease of comparison with the Ideal metal scaling relations.

4. In case of few doped systems with OOH adsorption, the adsorbate OOH breaks to form O* and OH. These systems are neglected from the scaling relation.
5. In few doped systems with O adsorption, the adsorbate O binds on the non-metal site (O) of the $Nb_{32-x}O_{80}$ surface. These systems are neglected from the scaling relation.

NOTE: *c_1 and c_2 represents site of adsorption of the ORR intermediates: on dopant and Nb site respectively.*

It is worth noting that under ORR reaction conditions, the realistic surface may not always be the pristine stoichiometric system. Ir-doped Nb_2O_5 systems has the pristine stoichiometric surface stable at the operating potential ($U=0.8V_{RHE}$)

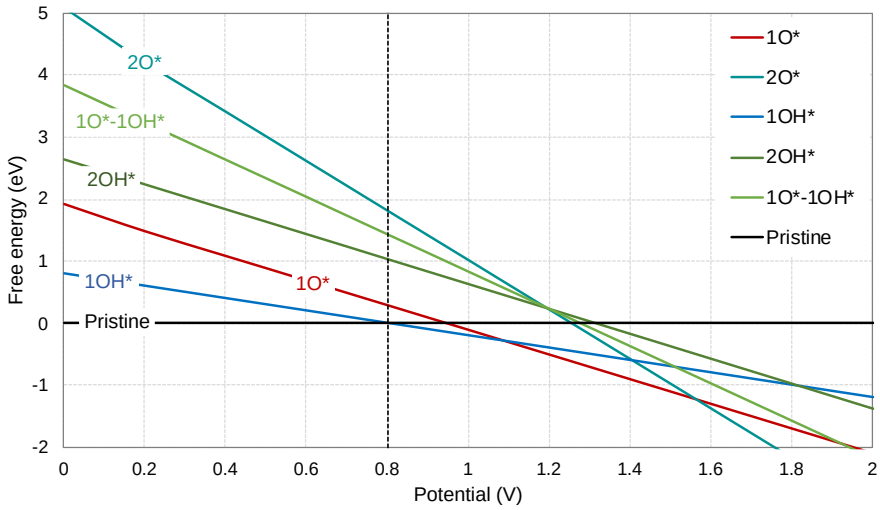

Fig S6 | Free energies versus applied potential (vs RHE) for different surface coverages on Ir-$Nb_{31}O_{80}$ (110) at pH = 0. *The * represent the adsorption site on Nb_2O_5 (110). The vertical dashed line 0.8 V shows the working potential for ORR.*

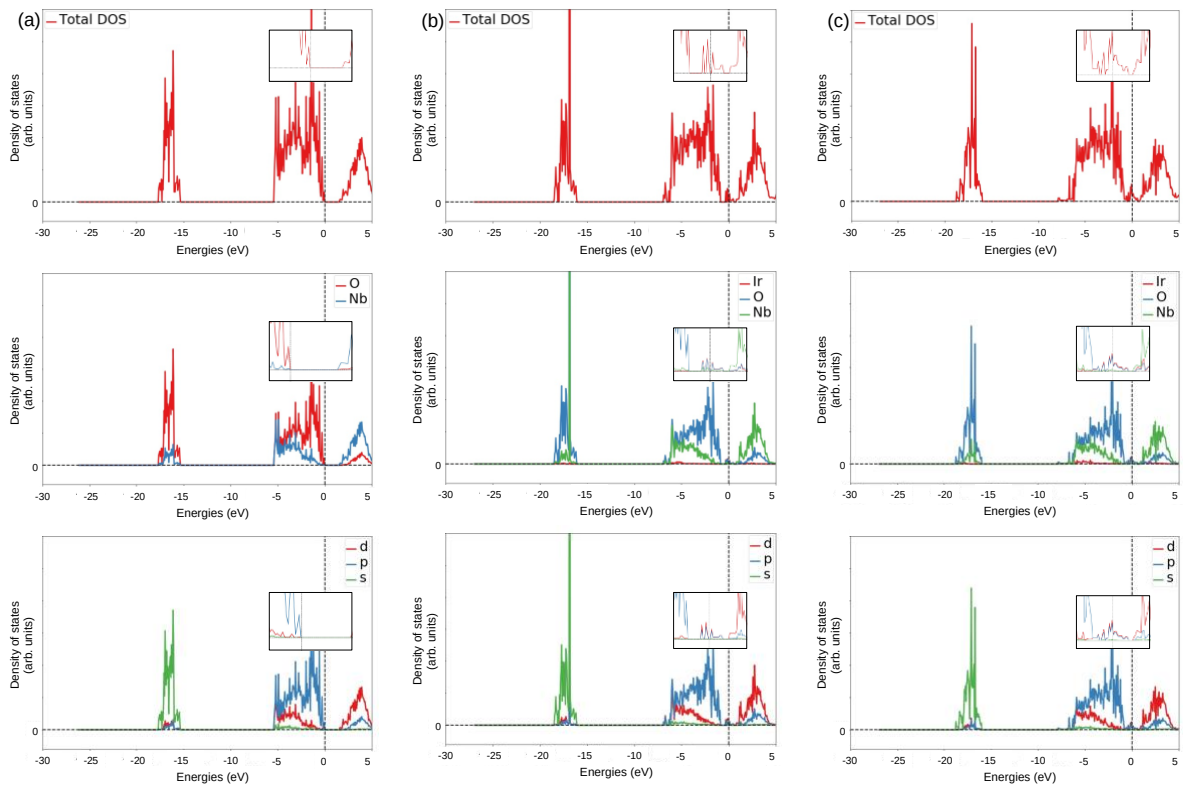

Fig S7 | Calculated TDOS and PDOS of (a) $Nb_{32}O_{80}$ (110), (b) Ir-$Nb_{31}O_{80}$ (c) 2Ir-$Nb_{30}O_{80}$. Fermi level (E_f) is represented by the vertical black dashed line.

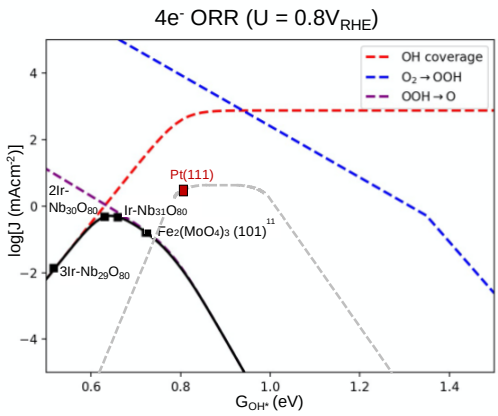

Fig S8 | Kinetic volcano model for the 4e- ORR process at 0.8 V_{RHE} for doped niobium oxide system (110) (solid black line) and TM systems (dashed grey line) using the kinetic model outlined in ref 11.

Red square marker represents Pt(111), ORR benchmark catalyst. Dashed lines indicate the activity of the 4e- ORR as solved by rate-determining step analysis with each potential rate-determining step corresponding to TMO system.

7. OH binding energy of IrO_2(110)

The most stable phase of IrO_2 (110) under reaction conditions is high coverage OH.

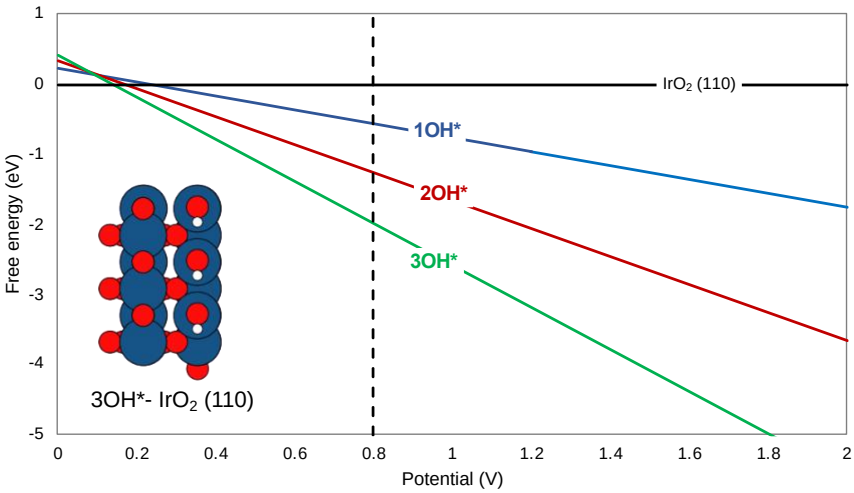

Fig S9 | Comparing free energies of different OH coverage surfaces sampled for IrO_2 (110) (pH = 0)

The differential binding energy of *OH on IrO_2 (110) can be given by:

$$G_b^{diff} = G_{nOH^*+slab} - (G_{(n-1)OH^*+slab} + G_{H_2O} - 0.5G_{H_2})$$

where n is the number of OH adsorbed on the slab, G_{nOH^*+slab} is the total energy of the surface with n adsorbed OH and is calculated relative to the H_2O (g) and H_2 (g).

Table S4 | Differential OH binding energy at high coverage on IrO_2 (110)

System	IrO_2 (110)	1OH*	2OH*	3OH*
Top view	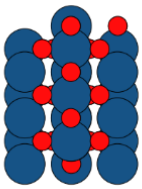	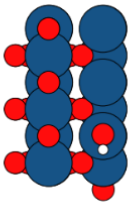	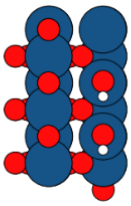	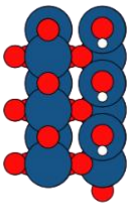
Electronic energy (eV)	-493.409	-504.665	-515.991	-527.344
E_b^{diff} (eV)		-0.087	-0.158	-0.186
G_b^{diff} (eV)		0.051	-0.021	-0.048

REFERANCES

[1] G. T. Kasun Kalhara Gunasooriya and Jens K. Nørskov, Analysis of Acid-Stable and Active Oxides for the Oxygen Evolution Reaction. *ACS Energy Lett.* 2020, **5**, 3778-3787.

[2] Joseph A. Gauthier, Colin F. Dickens, Leanne D. Chen, Andrew D. Doyle and Jens K. Nørskov, Solvation Effects for Oxygen Evolution Reaction Catalysis on IrO2(110). *J. Phys. Chem. C*, 2017, **121**, 11455.

[3] Zhenbin Wang, Ya-Rong Zheng, Ib Chorkendorff, and Jens K. Nørskov, Acid-Stable Oxides for Oxygen Electrocatalysis, *ACS Energy Lett.*, 2020, **5**, 2905.

[4] Olga Vinogradova, Dilip Krishnamurthy, Vikram Pande, and Venkatasubramanian Viswanathan, Quantifying Confidence in DFT-Predicted Surface Pourbaix Diagrams of Transition-Metal Electrode–Electrolyte Interfaces. *Langmuir*, 2018, **34**, 12259.

[5] Karsten Reuter and Matthias Scheffler, Composition, structure, and stability of RuO2(110) as a function of oxygen pressure. *Phys. Rev. B*, 2001, **65**, 035406-1.

[6] A. J. Bard and M. A. Fox, Artificial Photosynthesis: Solar Splitting of Water to Hydrogen and Oxygen. *Acc. Chem. Res*, 1995, **28**, 141.

[7] D. D. Wagman, W. H. Evans, V. B. Parker, R. H. Schumm, I. Halow, S. M. Bailey, K. L. Churney and R. L. Nuttall, The NBS tables of chemical thermodynamics properties: Selected Values for Inorganic and C1 and C2 Organic Substances in SI Units. 1982, **11**.

[8] W. H. Koppenol and J. Butler, Energetics of interconversion reactions of oxyradicals, *Advances in Free Radical Biology & Medicine*, 1985, **1**, 91.

[9] Allen J. Bard, Roger Parsons and Joseph Jordan, Standard Potentials in Aqueous Solution. (1st ed.). Routledge, 1985.

[10] David A. Armstrong, Robert E. Huie, Willem H. Koppenol, Sergei V. Lymar, Gábor Merényi, Pedatsur Neta, Branko Ruscic, David M. Stanbury, Steen Steenken and Peter Wardman, Standard Electrode Potentials Involving Radicals in Aqueous Solution: Inorganic Radicals. *Bioinorg. React. Mech.* 2013, **9**, 59.

[11] Hao Li, Sara Kelly, Dan Guevarra, Zhenbin Wang, Yu Wang, Joel A. Haber, Megha Anand, G.T. Kasun Kalhara Gunasooriya, Christina Susan Abraham, Sudarshan Vijay, John M. Gregoire and Jens K. Nørskov, Analysis of the Limitations in the Oxygen Reduction Activity of Transition Metal Oxide Surfaces. Nature Catal, 2021, 4, 463.